Cellular reprogramming for successful CNS axon regeneration is driven by a temporally changing cast of transcription factors

Authors: Sumona P. Dhara[1], Andrea Rau[2,3], Michael J. Flister[4], Nicole M. Recka[1], Michael D. Laiosa[3], Paul L. Auer[3], Ava J. Udvadia[1*]

[1]Department of Biological Sciences, University of Wisconsin-Milwaukee, Milwaukee, WI 53201, USA
[2]GABI, INRA, AgroParisTech, Universite Paris-Saclay, 78350, Jouy-en-Josas, France
[3]Joseph J Zilber School of Public Health, University of Wisconsin-Milwaukee, Milwaukee, WI 53201, USA
[4]Department of Physiology, Medical College of Wisconsin, Milwaukee, WI 53226, USA
[*]To whom correspondence may be addressed: audvadia@uwm.edu

Abstract

In contrast to mammals, adult fish display a remarkable ability to fully regenerate central nervous system (CNS) axons, enabling functional recovery from CNS injury. Both fish and mammals normally undergo a developmental downregulation of axon growth activity as neurons mature. Fish are able to undergo damage-induced “reprogramming” through re-expression of genes necessary for axon growth and guidance, however, the gene regulatory mechanisms remain unknown. Here we present the first comprehensive analysis of gene regulatory reprogramming in zebrafish retinal ganglion cells at specific time points along the axon regeneration continuum from early growth to target reinnervation. Our analyses reveal a regeneration program characterized by sequential activation of stage-specific pathways, regulated by a temporally changing cast of transcription factors that bind to stably accessible DNA regulatory regions. Strikingly, we also find a discrete set of regulatory regions that change in accessibility, consistent with higher-order changes in chromatin organization that mark (1) the beginning of regenerative axon growth in the optic nerve, and (2) the re-establishment of synaptic connections in the brain. Together, these data provide valuable insight into the regulatory logic driving successful vertebrate CNS axon regeneration, revealing key gene regulatory candidates for therapeutic development.

Keywords gene regulatory networks, optic nerve regeneration, chromatin accessibility, zebrafish

Introduction

Damage to nerves in the CNS as a result of disease or injury most often results in a permanent loss of function in humans. The loss of function stems from the failure of adult mammalian CNS neurons to support regenerative axon growth. In adult mammalian retinal ganglion cell (RGC) neurons, genetic and pharmacologic manipulations of neuron-intrinsic pathways have shown promise in activating a regenerative state after optic nerve injury [1-8]. However, even under these growth-enhanced conditions, regeneration mostly occurs only in a subset of RGCs [2], with the majority of axons rarely growing beyond a few millimeters. Furthermore, the regenerating axons frequently grow in an undirected manner, resulting in the “regenerated” axons terminating growth far from their appropriate brain targets [5,8,9]. As such, there remains a gap in our understanding of the genetic programs that drive RGC axon regeneration culminating in target re-innervation and recovery of visual function.

In contrast to mammals, zebrafish display a remarkable ability to spontaneously regenerate RGC axons. As opposed to regenerating axons in the growth-enhanced mouse models, regenerating axons in the zebrafish optic nerve successfully navigate across the chiasm and reinnervate target neurons in the optic tectum [10,11], ultimately leading to functional recovery [12]. It is well known that proteins regulating RGC axon growth and guidance in the developing visual system are highly conserved across vertebrate species, and are transcriptionally down-regulated once the mature circuitry has been established [13,14]. In addition, like mammals, optic nerve injury in adult zebrafish induces the expression of axon growth attenuators such as *socs3* in RGCs [6,15], suggesting that expression of such negative regulators of axon growth is a normal part of the regenerative program. One major difference in response to CNS axon injury between mammals and fish is the re-expression of a genetic program that promotes axon growth and guidance [16,17]. However, we and others have found that the regulation of axon growth-associated genes differs between development and regeneration [18-20]. Thus, the difference between mammals and vertebrate species capable of optic nerve regeneration is their ability to reprogram adult RGCs for axon growth in response to optic nerve injury.

It has been established that specific regeneration-associated gene expression changes in the adult zebrafish retina begin within the first day after optic nerve crush and persist through the re-innervation of the optic tectum [21]. What is less clear are the genome-wide changes in expression within the RGCs over time as they first grow toward their intermediate target of the optic chiasm

67 and then navigate toward their principal brain target, the optic tectum. Here we present the first
68 comprehensive analysis of gene expression changes (RNA-seq) and DNA regulatory element
69 accessibility (ATAC-seq) in zebrafish RGCs at specific time points along the axon regeneration
70 continuum from early growth to target reinnervation. Our analysis reveals that successful CNS
71 axon regeneration is regulated by stage-specific gene regulatory modules, and punctuated by
72 regeneration-associated changes in chromatin accessibility at stages corresponding to
73 axonogenesis and synaptogenesis. Together, these data suggest candidates for gene regulatory
74 targets for promoting successful vertebrate CNS axon regeneration.
75

76 # Results

77

78 **Stage-specific temporal changes in regeneration-associated gene expression**

79

80 We hypothesized that regeneration-associated gene expression changes in axotomized RGCs
81 would follow a temporal pattern corresponding to the changing requirements of axons as they
82 grow through different environments leading from retina to optic tectum. The timing of successful
83 axon regeneration after optic nerve crush in zebrafish is well characterized [10,11,22]. To achieve a
84 comprehensive picture of the genetic programming driving successful vertebrate CNS axon
85 regeneration, we used RNA-seq to identify changes in gene expression that accompanied axon
86 growth in regenerating RGCs at critical time points after optic nerve injury. We specifically
87 examined how transcript expression in naïve retinas compared with that in retinas dissected from
88 fish at 2, 4, 7, and 12 days post-injury (dpi). Based on the previously established regeneration
89 chronologies, our chosen time-points (Fig. 1A) correspond to following stages of optic nerve
90 regeneration: (1) axon growth past the site of injury toward the midline, (2) axon guidance across
91 the midline, (3) selection of axon targets within the brain, and (4) synaptogenesis in the optic
92 tectum [10,11,22].

93

94 Over the course of the first two weeks after optic nerve injury, we identified thousands of
95 transcripts that displayed regeneration-associated changes in expression with respect to the
96 baseline established from uninjured control retinas (Fig. 1B). Specifically, we found that 7,480
97 transcripts, roughly 19% of the retinal transcriptome, were differentially expressed in at least one
98 time point (Table S1). At time points corresponding to periods of regenerative axon growth from
99 retina to brain, 2-7 dpi, approximately three to four thousand transcripts were differentially

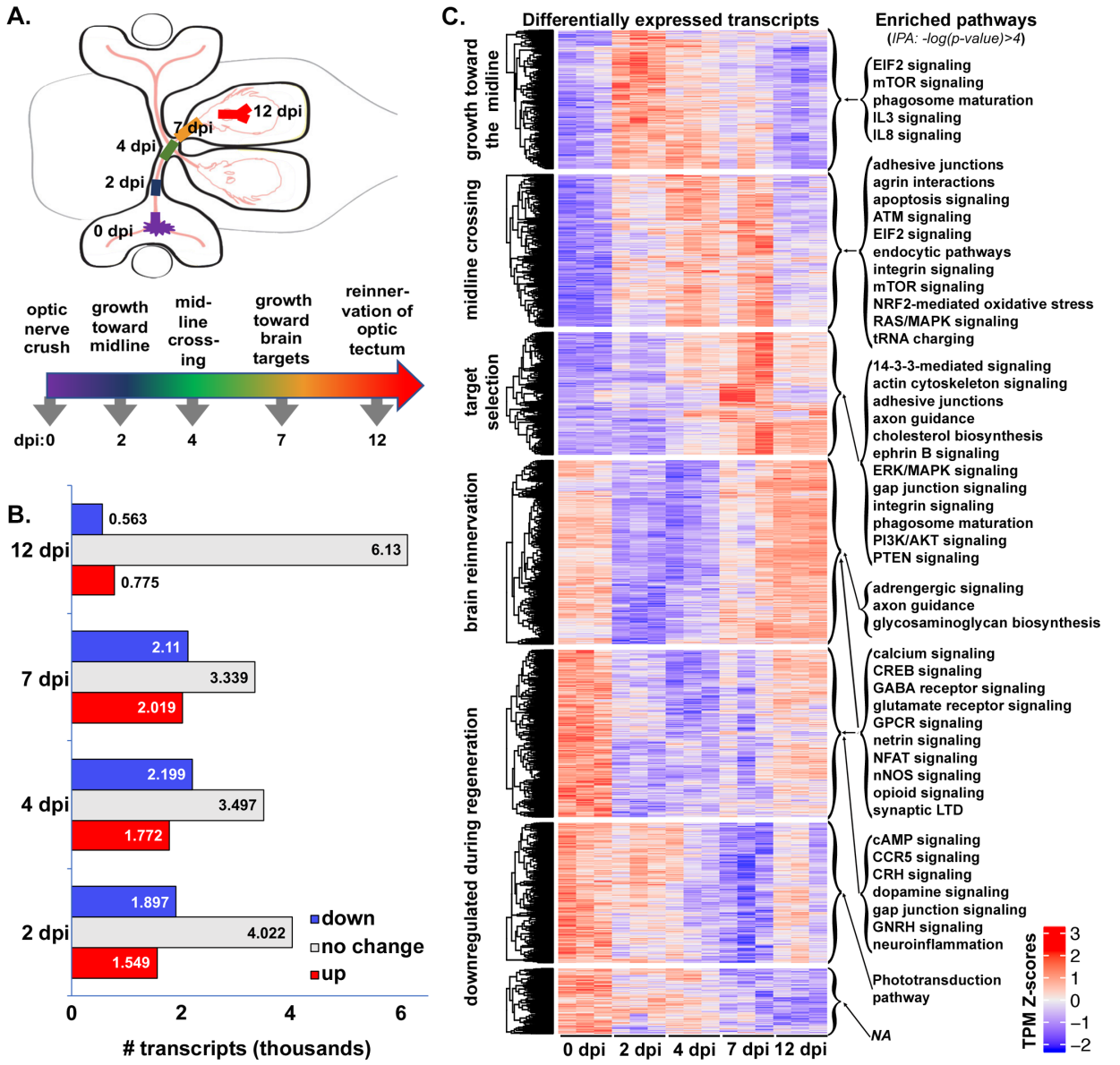

Fig.1. Regeneration-associated genes display stage-specific expression after optic nerve injury. (A) Schematic depicting stages of optic nerve regeneration from 0 – 12 days post-injury (dpi). (B) RNA-seq results generated from dissected retinas of adult zebrafish at 7-9 months of age. Transcripts from retinas dissected 2-12 days post optic nerve crush were compared with those from uninjured animals. Together, 7,080 transcripts were expressed at either higher (red = upregulated) or lower (blue = downregulated) levels in injured retina at 2, 4, 7, and/or 12 dpi when compared to control retinas (0 dpi), adjusted p values <0.05. (C) Temporally clustered transcripts demonstrate stage-specific enrichment of canonical pathways. Expression heatmaps produced from Z-scores (calculated using transcripts per million [TPM] estimates) of 4,614 differentially-expressed transcripts with adjusted p values <0.01. Mean normalized transcript counts were generated for each transcript across all samples at all time points. Each row represents a single transcript where each biological sample was compared to the mean, with red and blue indicating

standard deviation above and below the mean, respectively. Each column represents one of the three biological replicates for each time point. Genes within each cluster were analyzed by Ingenuity Pathway Analysis (IPA) using –log(*p-value*)>4, to identify pathways expressed in a regeneration stage-specific manner. *NA*, not applicable, indicates that no pathways we detected that met our significance threshold.

expressed at either higher or lower levels in injured retina when compared to control retinas. At 12 dpi, a time point corresponding to the re-establishment of synaptic connections in the tectum, the number of differentially expressed transcripts was lower, but still exceeded 1,000. These results reveal substantial changes in gene regulatory programming over the course of regeneration.

To visualize the temporal patterns of transcript expression over the full course of axon regeneration from retina to brain, we identified the timing of peak expression for each of the differentially expressed transcripts. This was achieved by calculating the Z-score for normalized transcript counts of individual transcripts in each sample, comparing against the mean derived from all replicates across all time points. Transcripts were then clustered into seven groups based on temporal patterning of Z-scores using the K-means algorithm (Fig. 1C, *Differentially expressed transcripts;* Table S2). As hypothesized, we detected distinct clusters of transcripts that were upregulated in response to injury that displayed peak expression at early, intermediate and late time points during regeneration. We also observed transcripts that were expressed at their highest levels in the uninjured retina and down-regulated early, midway, and later in the regenerative time course. Finally, we observed transcripts expressed in uninjured retina that were down-regulated early in regeneration, but displayed peak expression at the latest stage when regenerating fibers are in the process of synaptogenesis. The temporal patterning of the differentially regulated genes signifies a dynamic program of gene regulation that changes over the course of regeneration.

Given the temporal dynamics in gene expression associated with different stages of regeneration, we queried the data for evidence of stage-specific processes that drive successful regeneration. To identify canonical pathways represented by differentially expressed transcripts in each cluster, we conducted Ingenuity Pathway Analysis (Qiagen, Redwood City, CA). Enriched pathways, based on high stringency criteria (-log(*p*-value) > 4), were detected for six out of the seven temporal clusters (Fig. 1C, *Enriched pathways*; Table S3). We found little overlap in enriched pathways between the first three clusters, consistent with the idea of distinct processes active at different stages of regeneration.

149 Many of the enriched pathways at each time point were consistent with pathways previously
150 associated with axon regeneration and/or developmental wiring of the nervous system. For
151 example, the enrichment of pathways involved in mTOR and cytokine signaling early in
152 regeneration is consistent with results in mammalian models in which activation of these pathways
153 enhances axon growth and survival of RGCs after optic nerve crush [4,6,7]. Interestingly, PTEN
154 signaling pathway genes are enriched at an intermediate timepoint, consistent with the down-
155 regulation of mTOR observed as a normal part of the regenerative program in zebrafish [23]. At
156 timepoints associated with midline crossing and target selection, we also found an enrichment of
157 pathways involved in cytoskeletal regulation, cell-cell adhesion, and cell-substrate interactions,
158 as would be expected during axon growth and guidance. Simultaneously we see pathways
159 associated with neurotransmitter receptor signaling and G-protein coupled receptor signaling that
160 are downregulated during stages of axon growth and guidance, but are upregulated during
161 synaptogenesis. It should be noted that genes that are down regulated in response to injury and
162 re-expressed at later stages of regeneration may be contributing to the recently characterized
163 RGC dendritic remodeling that is necessary for successful regeneration [22]. We also observed
164 downregulation of neuroinflammatory pathways early in regeneration, which may contribute to
165 successful axon regeneration in zebrafish. Local inflammatory responses have previously been
166 demonstrated to accelerate axon growth, suggesting that there are specific inflammatory
167 pathways that promote regeneration and others that are inhibitory. Taken together, these results
168 demonstrate that post-injury transcriptional programming dictates the timing of stage-specific
169 processes associated with successful CNS axon regeneration.
170
171 **Changes in transcription factor expression, not chromatin accessibility, are associated**
172 **with temporal patterning of regeneration-associated transcripts**
173
174 In order to understand the regulatory system that guides the post-injury transcriptional program,
175 we identified putative regulatory DNA elements (promoters, enhancers and insulators) in RGCs
176 at different stages of regeneration. Assay for Transposase Accessible Chromatin sequencing
177 (ATAC-seq) [24], was employed to assess chromatin accessibility in nuclei isolated from RGCs.
178 Transgenic zebrafish expressing GFP under the regulation of the *gap43* promoter/enhancer [25]
179 enabled the specific isolation of RGCs from dissociated retinal cells at specific post-injury time
180 points using fluorescence activated cell sorting (FACS).
181

182 We detected over 40,000 peaklets representing consensus regions of accessible chromatin in
183 RGCs. The majority of peaks were located in intergenic regions, upstream or downstream from
184 annotated genes (Fig. 2A). Of the peaks located within genes, the vast majority were found within
185 non-coding sequences (Fig. 2A). Approximately 80% of accessible chromatin peaklets were found
186 distal to any annotated genes (Fig. S1), consistent with potential function as enhancers or
187 insulators. Correspondingly, the remaining approximately 20% of peaklets overlapped with 5'
188 UTRs or were located within 1kb of transcriptional start sites, consistent with potential function as
189 promoters (Fig. S1). These results are consistent with previous findings associating chromatin
190 accessible regions with proximal and distal gene regulatory elements [26].
191
192 Surprisingly, overall chromatin accessibility changed very little in response to optic nerve injury.
193 In fact, only 233 consensus regions of accessible chromatin (0.5%) were differentially accessible
194 in injured RGCs compared to control RGCs (Fig. 2B; Table S4). All but one of the differentially
195 accessible peaklets were found at 2 dpi or 12 dpi. Most of the differentially accessible peaklets at
196 2 dpi were differentially open, while most of those at 12 dpi were differentially closed. Furthermore,
197 the overlap between differentially accessible peaklets between the two time points consisted of
198 only two peaklets that were differentially open at both 2 and 12 dpi. Together these results suggest
199 that the accessibility of DNA regulatory elements in RGCs is relatively constant, even under
200 conditions that result in dynamic changes within the transcriptome. Thus, we predicted that the
201 availability of the transcription factors that bind to RGC DNA regulatory elements, rather than the
202 accessibility of the elements, must change over the course of regeneration.
203
204 To test the hypothesis that transcription factor expression is differentially regulated at different
205 stages of regeneration we identified transcription factors that displayed differential expression at
206 any point over the regeneration time course. We achieved this by cross-referencing our
207 transcriptomic data to a recently compiled list of human transcription factors [27] and used a global
208 differential (likelihood ratio test, LRT) to compile a list of transcription factor-encoding transcripts
209 associated with regeneration. We discovered 265 definitive transcription factor encoding genes
210 associated with 339 transcripts that were differentially expressed at one or more post-injury time
211 points (Fig. S2, Table S5). We further refined this list to 205 transcripts corresponding to 159
212 transcription factor encoding genes with defined DNA recognition motifs available in the JASPAR
213 [28] or CIS-BP [29] databases. As predicted, we found that differentially expressed transcription
214 factors display temporal clustering similar to that of the regeneration-associated differentially
215 expressed transcripts at large (Fig. 2C; Table S6).

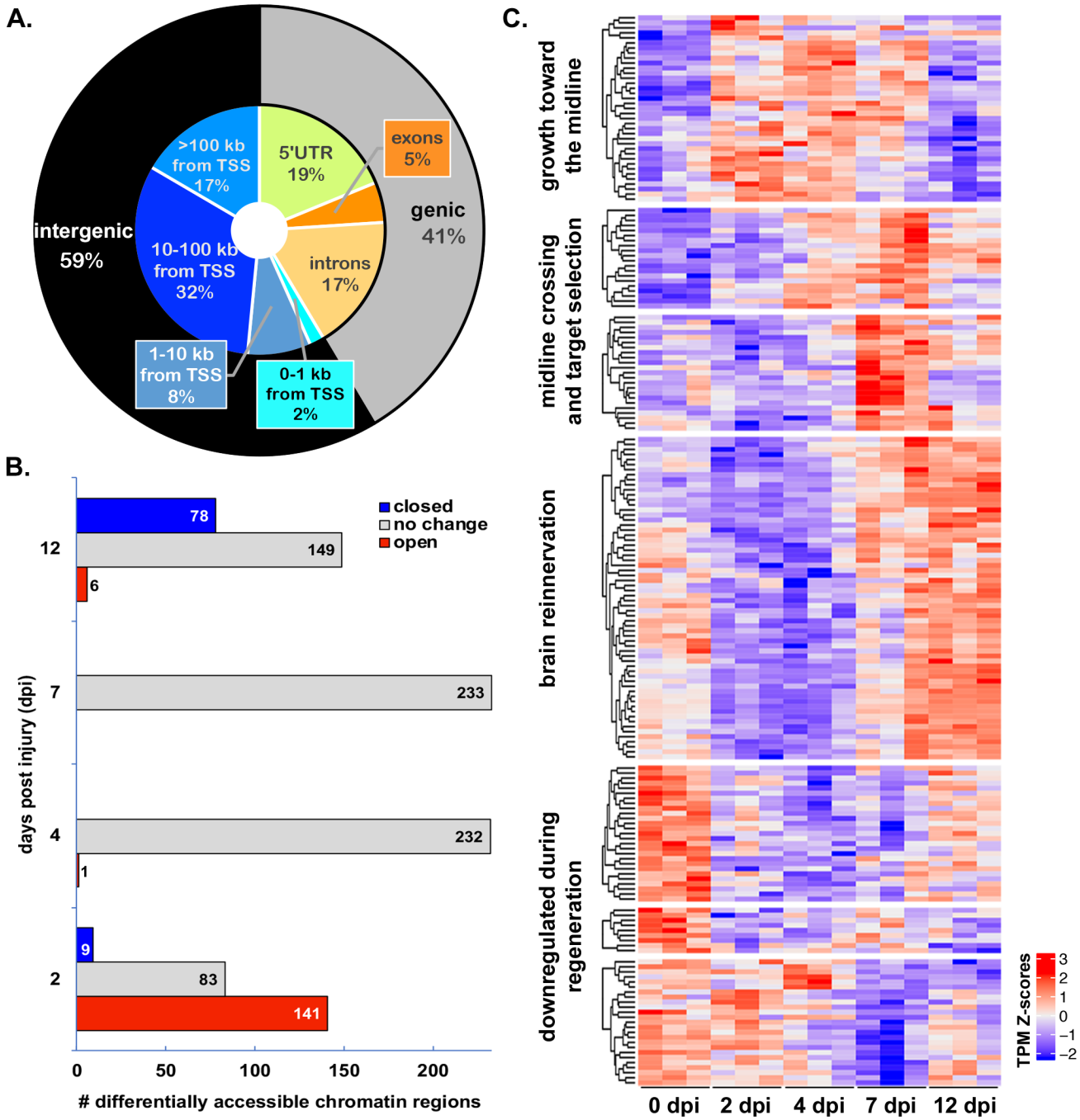

Fig. 2. Regeneration stage-specific gene expression changes are correlated with temporal changes in transcription factor expression rather than changes in chromatin accessibility. (A) Genomic distribution of 42,198 high confidence regions of accessible chromatin, identified using ATAC-seq on samples of RGCs isolated from control and regenerating retinas using fluorescence activated cell sorting (FACS). High confidence regions consist of 500 bp sequences surrounding peaklet summits with *p*-value < 10^{-10}. The genic region includes 5'-untranslated regions (UTR), exons and introns. The intergenic region consists of sequences found between annotated genes. (B) Most transcriptionally accessible regions do not change over the course of

226 regeneration when compared to uninjured control (0 dpi). Differentially accessible regions (233
227 total) were observed primarily at early (2 dpi) and late (12 dpi) stages of regeneration. (C)
228 Temporal progression of transcription factors characterizes the distinct stages of regeneration.
229 The expression heatmap of 205 differentially expressed transcripts represents 159 unique
230 transcription factor (TF) genes. TSS, transcriptional start site.
231

232 Thirty transcription factor families are represented among the transcription factors that were
233 differentially expressed during regeneration. Over half of the differentially expressed transcription
234 factors fall into four families (basic leucine zipper, basic helix-loop-helix, 2-Cys-2-His zinc finger,
235 and homeodomain). Each of these four families of transcription factors included representatives
236 with peak expression early, middle, and late in the regenerative process (Fig. 3), as well as those
237 whose expression was down-regulated during regeneration (Figs S3-S6). Within a given
238 transcription factor family, there are frequently binding motif similarities shared between
239 members. However, since transcription factors in these families may function as homo- and/or
240 heterodimers, their binding site affinity and transactivation ability may vary. Thus, a changing cast
241 of transcription factors would have the power to regulate the temporal progression of
242 regeneration-associated gene expression through a common set of accessible regulatory regions.

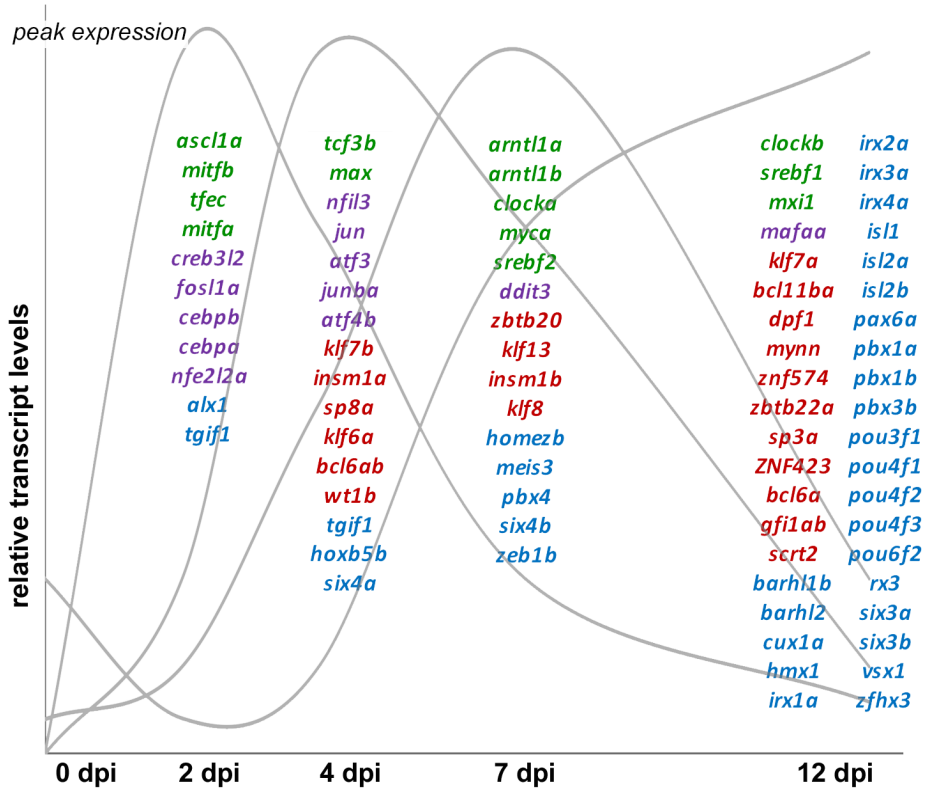

243
244

245 **Fig. 3. The majority of regeneration-associated transcription factors fall within four**
246 **transcription factor families.** Select transcription factor-encoding transcripts from the helix-loop-

247 helix (green), leucine zipper (purple), C2H2 zinc finger (red), and homeodomain families (blue)
248 transcription factor families grouped according to their peak expression (schematically
249 represented by grey curves). Although transcription factors from each of the families are
250 represented at different stages in regeneration, leucine zipper transcription factors appear more
251 prominent early in regeneration and homeodomain transcription factors are most prevalent later
252 in regeneration.
253

254 **Binding sites for differentially expressed transcription factors are enriched in inferred RGC**
255 **regulatory elements detected by chromatin accessibility**

256 To evaluate the potential for temporally expressed transcription factors to regulate stage-specific
257 regeneration-associated gene transcription, we used motif enrichment analysis [30]. For each
258 cluster of temporally expressed transcripts we identified potential regulatory elements in the form
259 of accessible chromatin peaklets that were proximal (peaklet center within ±1kb from transcription
260 start site) or distal (peaklet center within ±100 kb from transcription start site, but not proximal) to
261 the associated gene. Proximal and distal peaklet sequences were then queried for enrichment of
262 binding motifs of transcription factors with similar temporal expression profiles (Table S7). For
263 transcripts whose expression is upregulated early in regeneration (Fig. 1C, *growth toward the*
264 *midline* cluster), we found that motifs for 17 out of the 31 transcription factors queried were
265 enriched in the surrounding regions of accessible chromatin (Fig. 4A; Table S7). Motifs for the
266 zinc finger transcription factors, KLF6 and WT1, were detected in over 70% of both proximal and
267 distal elements. Including KLF6, a number of previously identified regeneration-associated
268 transcription factors are both upregulated early in optic nerve regeneration (Fig. 2C) and have
269 binding sites that are enriched within putative regulatory elements surrounding genes that are
270 also upregulated early in regeneration (Fig. 4A, Fig. 1C). Most notable among these are ASCL1
271 and the basic leucine zipper (bZIP) factors JUN, ATF3, FOSL1, and JUNB. In addition, other
272 transcription factors whose binding sites are enriched include those that have previously been
273 associated with axon growth in developing CNS neurons, such as WT1 and TCF3 [31,32].

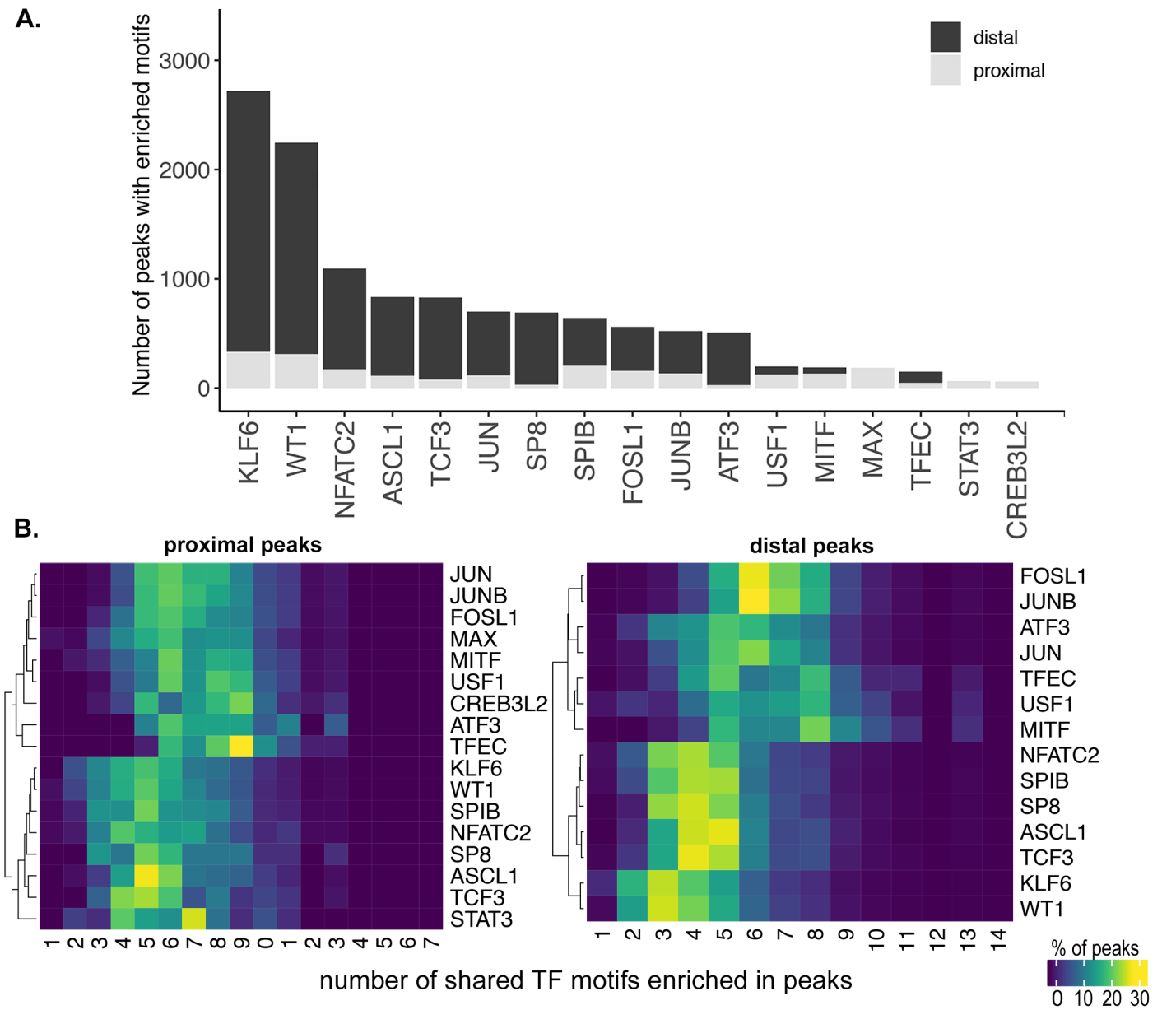
A.
Number of peaks with enriched motifs
3000
2000
1000
0
distal
proximal
KLF6
WT1
NFATC2
ASCL1
TCF3
JUN
SP8
SPIB
FOSL1
JUNB
ATF3
USF1
MITF
MAX
TFEC
STAT3
CREB3L2
B.
proximal peaks
distal peaks
JUN
JUNB
FOSL1
MAX
MITF
USF1
CREB3L2
ATF3
TFEC
KLF6
WT1
SPIB
NFATC2
SP8
ASCL1
TCF3
STAT3
FOSL1
JUNB
ATF3
JUN
TFEC
USF1
MITF
NFATC2
SPIB
SP8
ASCL1
TCF3
KLF6
WT1
1 2 3 4 5 6 7 8 9 0 1 2 3 4 5 6 7
1 2 3 4 5 6 7 8 9 10 11 12 13 14
number of shared TF motifs enriched in peaks
% of peaks
0 10 20 30

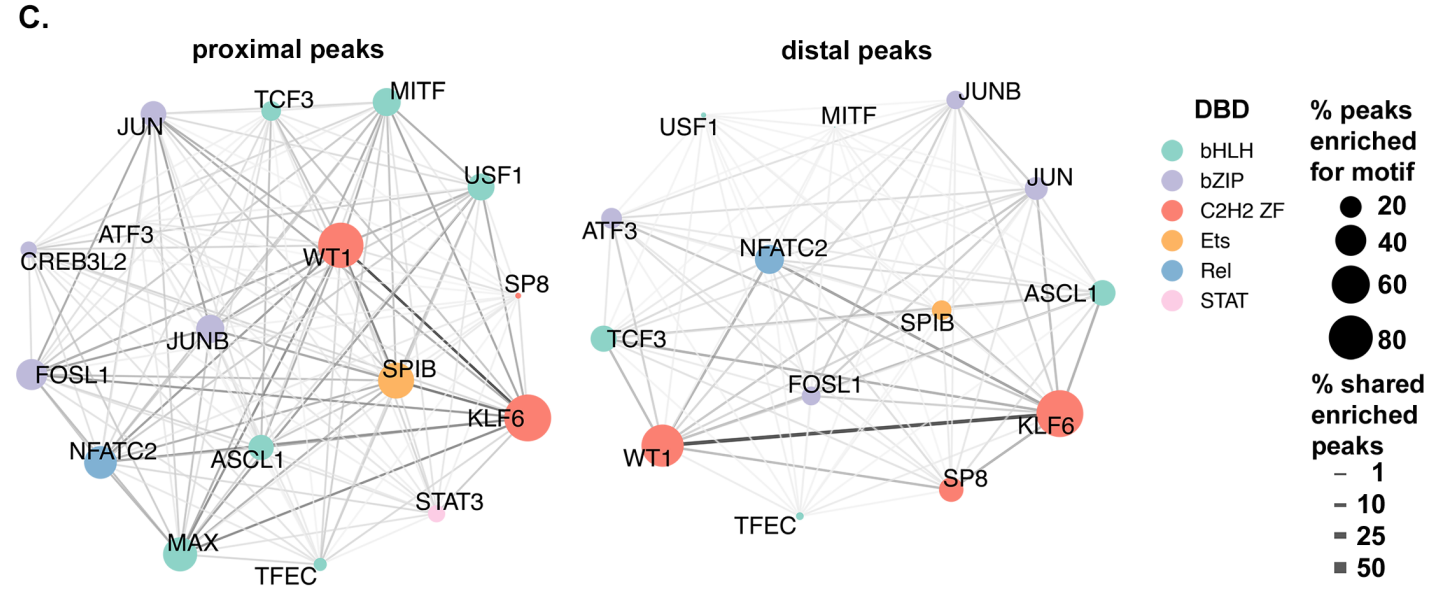
C.
proximal peaks
TCF3
MITF
JUN
USF1
ATF3
CREB3L2
WT1
SP8
JUNB
FOSL1
SPIB
KLF6
NFATC2
ASCL1
STAT3
MAX
TFEC
distal peaks
JUNB
USF1
MITF
JUN
ATF3
NFATC2
ASCL1
SPIB
TCF3
FOSL1
KLF6
WT1
SP8
TFEC
DBD
bHLH
bZIP
C2H2 ZF
Ets
Rel
STAT
% peaks enriched for motif
20
40
60
80
% shared enriched peaks
1
10
25
50

275
276 **Fig. 4. Potential regulatory interactions between regeneration-associated transcription**
277 **factors and putative promoters and enhancers.** (A) Stacked bar graph of number of peaks
278 enriched with transcription factor (TF) motif in the proximal (gray) and distal (black) sequences
279 for each TF in the cluster axon growth towards midline (cluster 1 in Fig.1). (B) Heat map of shared
280 TF motif enrichment in cluster1 accessible peaks. X-axis = number of shared TF motifs enriched
281 in peaks, Y-axis = TF. Heatmap colors based on % of total peaks enriched for given TF. (C) Pair-
282 wise co-occurrence of TF motifs found in the proximal and distal accessible regions surrounding
283 the differentially expressed transcripts of cluster 1. Node color corresponds to TF family based on
284 DNA-binding domain (DBD). bHLH, basic helix-loop-helix; bZIP, basic leucine zipper; C2H2 ZF,
285 two cys, two his zinc finger; Ets, E26 transformation-specific; Rel, member of NF-kB family; STAT,
286 signal transducer and activator of transcription. Node size corresponds to percentage of peaks
287 enriched for given TF. Edge thickness corresponds to % shared enriched peaks.
288
289 Promoters and enhancers rarely function in response to binding of single transcription factors.
290 This is due both to the propensity of transcription factors within the same family to dimerize, and
291 the existence of multiple transcription factor binding sites within a given promoter or enhancer. To
292 identify potential interactions between regeneration-associated transcription factors, we
293 quantified the frequency with which binding sites for differentially expressed transcription factors
294 co-occurred within putative regulatory elements. For example, although KLF6 and WT1 were the
295 most prevalent binding sites within both proximal and distal peaklets, the co-occurrence rate with
296 binding sites with other transcription factors present in this time window was among the lowest
297 (Fig. 4B). Within distal peaklets, KLF6 and WT1 binding sites frequently co-occurred with those
298 of 2-4 other factors (Fig. 4B, *distal peaks*). By comparison, binding motifs for FOSL1 and JUNB
299 displayed a high frequency of co-occurrence with binding sites for 6-7 other transcription factors
300 (Fig. 4B, *distal peaks*). A similar trend was observed among proximal peaklets, although the
301 differences were less marked (Fig. 4B, *proximal peaks*). These differences suggest the possibility
302 that binding site composition and potential transcription factor interactions may be distinguishing
303 characteristics of regeneration-associated promoters and enhancers.
304
305 We further quantified the frequency of specific co-occurring binding sites. The co-occurrence of
306 members of the same family was expected due to similarities in recognition sequence specificity.
307 This was observed most clearly in the frequency of shared enriched peaklets between KLF6 and
308 WT1 binding sites, and between the bZIP factors (Fig. 4C). However, we also observed frequent
309 co-occurrence of binding sites between members of different transcription families, most notably
310 ASCL1 and NFATC2. These results suggest numerous complex regulatory mechanisms that fine-
311 tune the expression of regeneration-associated genes including: (a) multiple within-family

312 interactions that influence binding site specificity and affinity, as well as transcriptional activity;
313 and (b) a variety of higher order multi-family complexes that may physically and/or functionally
314 interact.
315
316 **Regeneration-associated regulatory sequences target *jun* expression**
317 Although chromatin accessibility remains mostly stable in RGCs in response to optic nerve injury,
318 we detected a small number of DNA elements in which chromatin accessibility changed in
319 regenerating neurons compared to controls. Intriguingly, the few differentially accessible
320 chromatin peaklets were not evenly distributed across the time points. Instead, most of the
321 elements that became more accessible in response to injury did so at the earliest time point (2
322 dpi). This led us to postulate a role for these elements in triggering the regenerative growth
323 program. We hypothesized that transcription factors regulated by such elements would not only
324 regulate biological processes necessary for initiation of axon growth, but would also contribute to
325 the regulation of downstream transcription factors that in turn regulate subsequent phases of
326 regeneration.
327
328 In order to identify potential transcription factor targets of the regeneration-associated regulatory
329 elements, we ranked the differentially expressed transcription factor genes (Fig. 2C) on the basis
330 of their proximity to the differentially accessible chromatin regions. Surprisingly, *jun* was the only
331 regeneration-associated transcription factor encoding gene that was located within at least 100
332 kb of a differentially accessible chromatin region. In fact, the *jun* gene is flanked by three peaklets
333 that are differentially open at 2 dpi with respect to controls (Fig. 5A). One peaklet is centered at
334 148 bp upstream of the transcription start site within the putative promoter, and the two remaining
335 peaklets are located distally, approximately 3.6 kb downstream of the transcription start site. Motif
336 enrichment analysis of these sequences identified a motif for the JUN family of transcription
337 factors, suggesting the potential for autoregulation. We also scanned these sequences [33] for
338 motifs of other regeneration-associated transcription factors whose expression peaks early in
339 regeneration (Fig. 2C, Fig. 3). In addition to JUN binding sites, we found high-scoring matches for
340 KLF6, WT1, SP8, SPIB, FOSL1, JUNB, ATF3 and STAT3 motifs within these sequences.
341 Although JUN has long been associated with axon regeneration in both CNS and PNS [34-40],
342 mechanisms regulating its transcription in response to axonal injury are not well understood. Our
343 results indicate that differential activation of JUN early in regeneration is potentially a
344 consequence of increased accessibility of promoter and enhancer sequences to injury-induced
345 transcription factors.

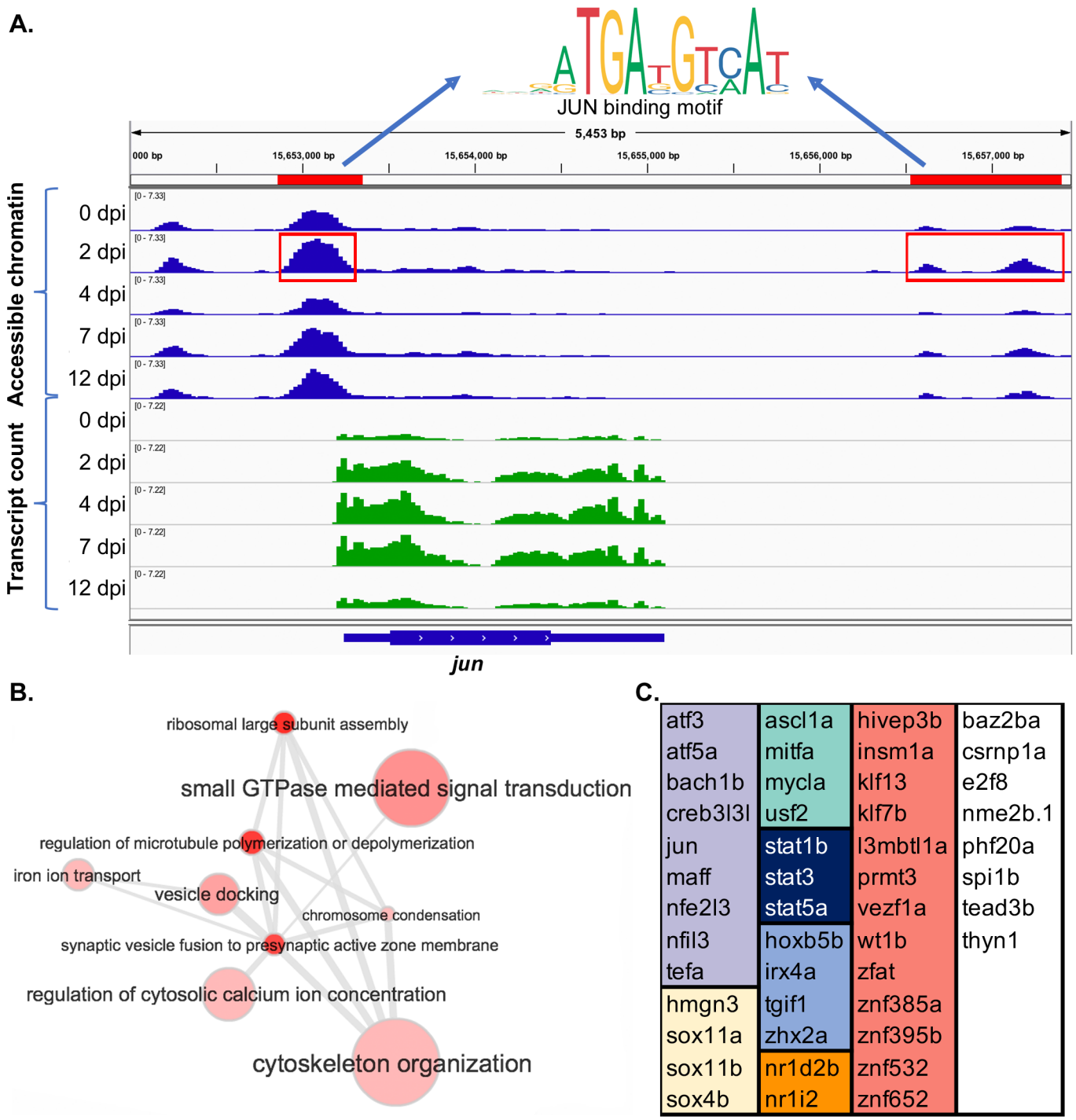

Fig. 5. *Jun* is a potential regulatory target of regeneration-associated promoters and enhancers.

(A) IGV browser screenshot displaying accessible chromatin sequence pileups (*blue*) and expressed sequence pileups (*green*) surrounding *jun* gene at 0, 2, 4, 7, and 12 dpi. Red bars and boxes indicate sequence determined to be differentially open at 2 dpi compared to control (0 dpi). Motif finding of sequences highlighted in red identified motifs corresponding to the JUN binding

site. (B) Gene ontology (GO) analysis of inferred targets of JUN suggests roles in calcium regulation, microtubule dynamics, and translation. GO terms corresponding to JUN target genes were summarized, clustered and visualized using REVIGO [36]. Node size corresponds to GO term frequency. Similar GO terms are linked by edges whose thickness corresponds to degree of similarity. (C) Inferred targets of JUN include 47 regeneration-associated TF genes. TF genes are grouped by transcription factor family: *violet*, leucine zipper; *yellow*, HMG/sox; *green*, helix-loop-helix; *dark blue*, STAT; *light blue*, hox; *orange*, nuclear receptor; *red*, C2H2 zinc finger; *white*, includes members of the AT hook, E2F, Ets, MBD, and TEA families as well as factors with uncategorized DNA binding domains.

We next analyzed the putative target genes of JUN for specific functional roles in the regenerative process. Putative JUN targets were identified based on our previous motif analysis (Fig. 3). Gene ontology analysis revealed a number of enriched biological processes consistent with a role for JUN in initiating axon regeneration (Table S8). The most significantly enriched terms include those involved in the regulation of microtubule dynamics and organization of the cytoskeleton, as well as those associated with small GTPase mediated signal transduction (Rho and Rab), and calcium regulation (Fig. 5B). The biological processes associated with potential JUN targets are a distinct subset of those associated with the larger list of all regeneration-associated genes in the same temporal clusters (Table S9). In the list of inferred JUN transcriptional targets, we also identified 47 regeneration-associated transcription factor encoding genes (Fig. 5C). This list includes 60% of the regeneration-associated transcription factors found in the first two temporal clusters (Fig. 1C). Thus, JUN has the potential for promoting and sustaining the regenerative program through activation of multiple downstream regeneration-associated transcription factors. Together the putative JUN targets suggest a central role for JUN in initiating and supporting successful CNS axon growth.

Discussion

We have conducted the first combined temporal analysis of chromatin accessibility and transcriptomic changes that accompanies successful optic nerve regeneration. By identifying accessible regulatory elements, coupled with stage-specific transcription factor availability and downstream targets, these results provide a roadmap to the gene regulatory networks governing successful optic nerve regeneration. A major conclusion of this study is that temporally distinct functional modules are regulated by a dynamic cast of regeneration-associated transcription factors binding to regulatory elements that are accessible in naïve and regenerating RGCs. Many

389 of the transcription factors have previously established roles in axon regeneration, while the roles
390 of many more remain to be functionally validated. More than half of these regeneration-associated
391 transcription factors fall into four transcription factor families, each with 25 or more members
392 whose peak expression varies in a stage-specific manner. This is the first study that establishes
393 a temporal hierarchy for regeneration-associated transcription factors based on expression
394 patterns of transcription factors, target genes, and binding site accessibility. Future studies that
395 use mass spectrometry approaches to identify stage-specific binding complexes could determine
396 how the relative stoichiometry of individual factors at different stages of regeneration impacts
397 complex formation and transcriptional activity.
398
399 Interestingly, the number of regeneration-associated changes in regulatory element accessibility
400 are more than an order of magnitude less frequent in number than regeneration-associated
401 changes in gene expression. Furthermore, the differentially accessible elements are almost
402 exclusively found at 2 dpi and 12 dpi, our earliest and latest timepoints, respectively. Based on
403 the timing and limited number of differentially accessible elements, we postulated a role for these
404 elements in triggering transcriptional programs for axon regrowth, and synaptogenesis. We
405 hypothesize at least two mechanisms by which this could occur: (i) The elements may be
406 responsible for initiating the expression of key regeneration-associated transcription factors,
407 which would subsequently regulate other factors in the hierarchy; and (ii) The elements may serve
408 to shift the higher order chromatin structure to reposition enhancers and promoters for the
409 transitions necessary in adult RGCs to reinitiate programs for axonogenesis (2 dpi), and and
410 synaptogenesis (12 dpi).
411
412 Our data contain evidence supporting both hypotheses. Supporting the first hypothesis, we find
413 that the gene encoding transcription factor JUN is flanked by promoter and distal enhancer
414 elements that increase in accessibility during axon regeneration. In fact, JUN involvement in such
415 epigenetic activation of pro-regenerative genes in response to axon injury was suggested in a
416 recent review [41]. Supporting our second hypothesis, we find that roughly half the differentially-
417 accessible regions at both early and late times are enriched in CTCF binding sites. CTCF is a
418 transcription factor that has recently been implicated in mediating chromatin looping and marking
419 the boundaries of topologically associating domains [42]. A logical next step would be to functionally
420 validate interactions between the predicted *jun* promoter and enhancers, as well as additional
421 long-range regulatory interactions between stably and differentially accessible elements using
422 chromatin capture and genome editing technologies.

423

424 The combination of gene expression and genomic accessibility over time provides a powerful
425 model of axon regeneration-associated gene regulatory networks. As with any modeling
426 approach, empirical testing and improved technology are expected to refine and strengthen the
427 predictive power of the model. For example, current methods for associating enhancers with
428 target genes will improve with the functional testing of these types of interactions as described
429 above. Another potential caveat of these studies is that the transcriptomic analysis were carried
430 out on whole retinas, rather than FACS-sorted RGCs that were utilized in the chromatin
431 accessibility. Because RGCs are the only cells directly injured by optic nerve crush, a comparison
432 of gene expression between injured and uninjured retina should primarily reflect changes in
433 RGCs. Yet, it is possible that some of the transcriptomic changes detected may be occurring in
434 other cells within the injured retina, such as infiltrating microglia or retinal neurons connected to
435 RGCs. However, we find good concordance between our transcriptomic results and microarray
436 studies based on RNA extracted from RGCs isolated by laser capture microdissection [17]. In
437 addition, our temporal approach using RNA-seq has greatly expanded detection of regeneration-
438 associated changes in gene expression over previous studies. We anticipate that functional
439 testing of the networks predicted by this model will substantially expand our understanding of the
440 molecular mechanisms governing successful optic nerve regeneration.

441

442 In summary, these data provide a roadmap for the identification of key combinations of
443 transcription factors necessary to reprogram adult RGCs for optic nerve regeneration. Similar
444 approaches have been employed to discover transcription factors necessary for direct
445 reprogramming of somatic cells to produce motor neurons [43]. However, to our knowledge, this is
446 the first gene regulatory network analysis of optic nerve regeneration that couples temporal
447 analysis of gene expression with the identification of putative regulatory interactions based on
448 chromatin accessibility and transcription factor expression. We expect that these findings may be
449 applicable to neurons in other regions of the CNS undergoing regenerative axon growth, such as
450 the spinal cord and brain. In order to facilitate comparisons between our data and those derived
451 from other regenerative models, we have created an interactive web application (*Regeneration*
452 *Rosetta;* http://ls-shiny-prod.uwm.edu/rosetta/) [44]. This app enables users to upload a gene list of
453 interest from any Ensembl-supported species and determine how those genes are expressed and
454 potentially regulated in the context of optic nerve regeneration. Such cross-species and cross-
455 system analyses will facilitate identification of novel pathways specifically associated with
456 successful CNS regeneration.

457

458 ## Materials and Methods

459 Detailed methods can be found in supplementary information.

460

461 **Zebrafish husbandry and optic nerve injury**

462

463 Zebrafish husbandry and all experimental procedures were approved by the *Institutional Animal*
464 *Care and Use Committee* (IACUC) and carried out in accordance with the relevant guidelines and
465 regulations thereof. The Tg (Tru.gap43:egfp) mil1 (aka fgap43:egfp) transgenic
466 line and Ekkwill wild type strain were maintained as previously described [25]. Optic nerve crush
467 (ONC) lesions were performed on adult zebrafish, 7-9 months of age, as previously described [21].

468

469 **RNA-seq data generation**

470

471 RNA was extracted and purified from retinas dissected from naïve (0 dpi) and regenerating adult
472 fish at 2, 4, 7, and 12 dpi. RNA was extracted using the RNeasy Micro kit (Qiagen) and
473 concentrated using the RNA Clean & Concentrator kit (Zymo). Three replicates were obtained
474 for each time point. Whole retinas were used for transcriptomic studies because the quality of the
475 RNA was much higher from whole retina. cDNA libraries were generated for each RNA sample
476 using Tru-Seq Stranded Total & mRNA Sample Prep Kits, (Illumina 20020595). Each cDNA library
477 was indexed for multiplexing and subsequently sequenced on four lanes of the Illumina
478 Hiseq2000. Libraries were sequenced at 50 bp, 30–40 million paired-end reads/sample.

479

480 After merging technical replicates of RNA-seq samples across lanes, adapter sequences were
481 trimmed (TrimGalore, v0.4.4), sequence quality was validated (FastQC, v0.11.5), and transcript
482 abundance was estimated using 500 bootstrap samples (Kallisto (v0.42.4) [45].

483

484

485 **ATAC-seq data generation**

486

487 Chromatin was extracted from nuclei isolated from purified populations of RGCs. Retinas were
488 dissected from naïve and regenerating fgap43:egfp fish as described above, and enzymatically
489 dissociated for FACS. Cell suspensions were pooled from multiple retinas at each time point (0

490 dpi, 8-10 retina; 2, 4, 7, and 12 dpi, 4-6 retinas), and sorted for RGCs expressing GFP using a
491 Becton Dickinson FACSAria™ III sorter. Although levels of endogenous Gap43 are low in the
492 naïve adult retina, the GFP transgene tends to be long lived and is detectable by FACS at levels
493 that are above background but below the level of visual detection. This enabled us to sort RGCs
494 from naïve retinas since new RGCs that continue to be added throughout the life of the animal
495 and low-levels of GFP persist in RGCs even after these new RGCs have established connections
496 in the tectum. However, we required twice the number of naïve retinas compared with injured
497 retinas to accumulate the 50,000 RGCs required for constructing the ATAC-seq libraries. Three
498 replicates of pooled cells were collected for each time point. ATAC-seq libraries were prepared
499 using the Tn5 transposase system (Nextera DNA library kit, Illumina, FC-121–1030) as previously
500 described [46], and purified using DNA Clean & Concentrator kit (SKU: ZD5205, Zymo).
501
502 Prior to running the full sequence, sequencing depth was estimated and one sample was below
503 the cut-off criteria and therefore omitted. The remaining fourteen samples were indexed for
504 multiplexing and subsequently sequenced on four lanes of the Illumina Hiseq2000Data at 50 bp
505 reads to obtain approximately 25 million paired-end reads/samples.
506
507 After merging technical replicates of ATAC-seq samples across lanes, adapter sequences were
508 trimmed (TrimGalore, v0.4.4) and sequence quality was validated (FastQC, v0.11.5). Reads were
509 aligned to GRCz10 as well as the transgene sequence (BWA-MEM (v0.7.9a-r786) [47]). Duplicate
510 and multiple mapped reads were removed using samtools (v1.6) [48]. After concatenating aligned
511 reads across all replicates and time points, MACS2 [49] (v2.1.1.20160309) was used to call peaks
512 from aligned reads. Only peaks with a p-value < 10-10 were retained for subsequent analyses.
513 For each remaining subpeak summit, a 500bp “peaklet” interval was defined using
514 GenomicRanges (v1.30.3) [50]. We refer to these peaklets as consensus regions of accessible
515 chromatin. Open chromatin in each replicate of each time point was then quantified using DiffBind
516 (v2.6.6, default parameters) by counting the number of overlapping reads for each retained
517 peaklet.
518
519 We used motif analysis to determine potential binding sites of differentially expressed transcription
520 factors within regions of accessible chromatin identified by ATAC-seq. Motif enrichment and
521 discovery was carried out within the MEME Suite of motif-based sequence analysis tools (version
522 5.0.3) [51].
523

524

525 **Statistical analysis of RNA-seq and ATAC-seq data**

526

527 Following pseudoalignment and quantification of transcripts, differentially expressed transcripts
528 were identified using Sleuth (v0.29.0) [52], either comparing each time point post injury (2, 4, 7, 12
529 dpi) to the initial time point (0dpi) using a Wald test statistic or using a likelihood ratio test (LRT)
530 to compare the full model with a time factor versus the null model, controlling the false discovery
531 rate (FDR) at 5% [53]. Expression heatmaps (based on Z-scores calculated using log transcripts
532 per million [TPM] estimates) were produced using ComplexHeatmap [54] (v1.17.1), where transcript
533 clusters were identified using the K-means algorithm, and hierarchical clustering (Euclidean
534 distance, complete linkage) was used to cluster rows. The Ingenuity Pathway Analysis tool
535 (Qiagen, Redwood City, CA, USA) was used to analyze enrichment of molecular and functional
536 gene networks within the differentially expressed gene sets (FDR<0.05) at each time point after
537 injury (2, 4, 7, 12 dpi) compared with the initial time point (0dpi).

538

539 After quantifying peaklet accessibility, DESeq2 (v1.18.1) [55] was used to identify differentially
540 accessible peaklets in an analogous manner to the RNA-seq analysis described above. Peaklets
541 with FDR-controlled p-values < 0.05 in one of the four comparisons were considered to be
542 differentially accessible. ChIPpeakAnno (v3.12.7) [56], the danRer10.refGene UCSC annotation
543 package (v3.4.2), and AnnotationHub (v2.10.1) were used to annotate peaklets with genes.
544 Specifically, non-exonic (i.e., not overlapping exons by more than 50bp) peaklets overlapping a
545 transcription start site (TSS) or within 1kb of a TSS were considered to represent proximal peaks,
546 whereas those greater than 1kb but less than 100kb of a TSS were considered distal peaks. All
547 statistical analyses were performed in R (v3.4.3). Integrative Genome Viewer (IGV) was used to
548 visualize RNA-seq and ATAC-seq alignments [57].

549

550

551 **Acknowledgements**

552 We thank the UWM High Performance Computing (HPC) Service for computing resources used
553 in this work. We are grateful to Heather Leskinen and Sarah Sarich for comments on the
554 manuscript and edits to the material and methods. We wish to thank the University of Wisconsin
555 Biotechnology Center DNA Sequencing Facility, Madison for providing RNA and ATAC sample
556 sequencing facilities. We gratefully acknowledge support from the Research Growth Initiative
557 Grant RGI (to A.J.U. and P.L.A.), University of Wisconsin-Milwaukee. A.R. was supported by the

AgreenSkills+ fellowship program, which received funding from the EU's Seventh Framework Program under grant agreement number FP7-609398 (AgreenSkills+ contract). S.D. was supported by the Clifford H. Mortimer Award, University of Wisconsin-Milwaukee

Author Contributions

AJU was responsible for the conception and design of the work. SPD, NMR, MDL and AJU contributed to tissue processing and sample collection for nucleic acid libraries. AR and PLA were responsible for the bioinformatics and statistical analyses of the RNA-seq and ATAC-seq data. MJF conducted the pathway analysis. SPD, AR, PLA and AJU contributed to the interpretation of the data, preparation of the figures, and writing of the manuscript. All authors reviewed the manuscript.

Competing Interests

The authors declare no competing interests.

Data availability

Raw sequencing files for the RNA-seq and ATAC-seq data will be submitted upon publication to the Sequence Read Archive (SRA). All scripts used to process and analyze the RNA-seq and ATAC-seq data may be found at https://github.com/andreamrau/OpticRegen_2019. The *Regeneration Rosetta* app may be accessed at http://ls-shiny-prod.uwm.edu/rosetta/, and all associated source files for creating the app may be found at https://github.com/andreamrau/rosetta.

References

1 Belin, S. *et al.* Injury-induced decline of intrinsic regenerative ability revealed by quantitative proteomics. *Neuron* **86**, 1000-1014, doi:10.1016/j.neuron.2015.03.060 (2015).

2 Duan, X. *et al.* Subtype-specific regeneration of retinal ganglion cells following axotomy: effects of osteopontin and mTOR signaling. *Neuron* **85**, 1244-1256, doi:10.1016/j.neuron.2015.02.017 (2015).

3 Leibinger, M. *et al.* Boosting central nervous system axon regeneration by circumventing limitations of natural cytokine signaling. *Mol Ther* **24**, 1712-1725, doi:10.1038/mt.2016.102 (2016).

4 Park, K. K. *et al.* Promoting Axon Regeneration in the Adult CNS by Modulation of the PTEN/mTOR Pathway. *Science* **322**, 963-966, doi:10.1126/science.1161566 (2008).

592 5 Pernet, V. *et al.* Long-distance axonal regeneration induced by CNTF gene transfer is
593 impaired by axonal misguidance in the injured adult optic nerve. *Neurobiol Dis* **51**, 202-
594 213, doi:10.1016/j.nbd.2012.11,011 (2013).

595 6 Smith, P. D. *et al.* SOCS3 deletion promotes optic nerve regeneration in vivo. *Neuron*
596 **64**, 617-623, doi:10.1016/j.neuron.2009.11.021 (2009).

597 7 Sun, F. *et al.* Sustained axon regeneration induced by co-deletion of PTEN and SOCS3.
598 *Nature* **480**, 372-U125, doi:10.1038/nature10594 (2011).

599 8 Trakhtenberg, E. F. *et al.* Zinc chelation and Klf9 knockdown cooperatively promote
600 axon regeneration after optic nerve injury. *Exp Neurol* **300**, 22-29,
601 doi:10.1016/j.expneurol.2017.10.025 (2018).

602 9 Luo, X. T. *et al.* Three-dimensional evaluation of retinal ganglion cell axon regeneration
603 and pathfinding in whole mouse tissue after injury. *Exp Neurol* **247**, 653-662,
604 doi:10.1016/j.expneurol.2013.03.001 (2013).

605 10 Diekmann, H., Kalbhen, P. & Fischer, D. Characterization of optic nerve regeneration
606 using transgenic zebrafish. *Front Cell Neurosci* **9**, doi:ARTN 118,
607 10.3389/fncel.2015.00118 (2015).

608 11 Lemmens, K. *et al.* Matrix metalloproteinases as promising regulators of axonal regrowth
609 in the injured adult zebrafish retinotectal system. *Journal of Comparative Neurology* **524**,
610 1472-1493, doi:10.1002/cne.23920 (2016).

611 12 Kaneda, M. *et al.* Changes of phospho-growth-associated protein 43 (phospho-GAP43)
612 in the zebrafish retina after optic nerve injury: a long-term observation. *Neurosci Res* **61**,
613 281-288, doi:10.1016/j.neures.2008.03.008 (2008).

614 13 Erskine, L. & Herrera, E. Connecting the retina to the brain. *ASN Neuro* **6**,
615 doi:10.1177/1759091414562107 (2014).

616 14 Skene, J. H. Axonal growth-associated proteins. *Annu Rev Neurosci* **12**, 127-156,
617 doi:10.1146/annurev.ne.12.030189.001015 (1989).

618 15 Elsaeidi, F., Bemben, M. A., Zhao, X. F. & Goldman, D. Jak/Stat signaling stimulates
619 zebrafish optic nerve regeneration and overcomes the inhibitory actions of Socs3 and
620 Sfpq. *J Neurosci* **34**, 2632-2644, doi:10.1523/JNEUROSCI.3898-13.2014 (2014).

621 16 Bernhardt, R. R., Tongiorgi, E., Anzini, P. & Schachner, M. Increased expression of
622 specific recognition molecules by retinal ganglion cells and by optic pathway glia
623 accompanies the successful regeneration of retinal axons in adult zebrafish. *J Comp*
624 *Neurol* **376**, 253-264, doi:10.1002/(SICI)1096-9861(19961209)376:2<253::AID-
625 CNE7>3.0.CO;2-2 (1996).

626 17 Veldman, M. B., Bemben, M. A., Thompson, R. C. & Goldman, D. Gene expression
627 analysis of zebrafish retinal ganglion cells during optic nerve regeneration identifies

KLF6a and KLF7a as important regulators of axon regeneration. *Dev Biol* **312**, 596-612, doi:10.1016/j.ydbio.2007.09.019 (2007).

18 Kusik, B. W., Hammond, D. R. & Udvadia, A. J. Transcriptional regulatory regions of gap43 needed in developing and regenerating retinal ganglion cells. *Dev Dyn* **239**, 482-495, doi:10.1002/dvdy.22190 (2010).

19 Senut, M. C., Gulati-Leekha, A. & Goldman, D. An element in the alpha1-tubulin promoter is necessary for retinal expression during optic nerve regeneration but not after eye injury in the adult zebrafish. *J Neurosci* **24**, 7663-7673, doi:10.1523/JNEUROSCI.2281-04.2004 (2004).

20 Udvadia, A. J., Koster, R. W. & Skene, J. H. GAP-43 promoter elements in transgenic zebrafish reveal a difference in signals for axon growth during CNS development and regeneration. *Development* **128**, 1175-1182 (2001).

21 Bormann, P., Zumsteg, V. M., Roth, L. W. A. & Reinhard, E. Target contact regulates GAP-43 and alpha-tubulin mRNA levels in regenerating retinal ganglion cells. *J Neurosci Res* **52**, 405-419, doi:10.1002/(Sici)1097-4547(19980515)52:4<405::Aid-Jnr4>3.0.Co;2-D (1998).

22 Beckers, A. *et al.* An Antagonistic Axon-Dendrite Interplay Enables Efficient Neuronal Repair in the Adult Zebrafish Central Nervous System. *Mol Neurobiol* **56**, 3175-3192, doi:10.1007/s12035-018-1292-5 (2019).

23 Diekmann, H., Kalbhen, P. & Fischer, D. Active mechanistic target of rapamycin plays an ancillary rather than essential role in zebrafish CNS axon regeneration. *Front Cell Neurosci* **9**, doi:ARTN 251, 10.3389/fncel.2015.00251 (2015).

24 Buenrostro, J. D., Giresi, P. G., Zaba, L. C., Chang, H. Y. & Greenleaf, W. J. Transposition of native chromatin for fast and sensitive epigenomic profiling of open chromatin, DNA-binding proteins and nucleosome position. *Nat Methods* **10**, 1213-1218, doi:10.1038/nmeth.2688 (2013).

25 Udvadia, A. J. 3.6 kb Genomic sequence from Takifugu capable of promoting axon growth-associated gene expression in developing and regenerating zebrafish neurons. *Gene Expr Patterns* **8**, 382-388, doi:10.1016/j.gep.2008.05.002 (2008).

26 Daugherty, A. C. *et al.* Chromatin accessibility dynamics reveal novel functional enhancers in C. elegans. *Genome Res* **27**, 2096-2107, doi:10.1101/gr.226233.117 (2017).

27 Lambert, S. A. *et al.* The Human Transcription Factors. *Cell* **172**, 650-665, doi:10.1016/j.cell.2018.01.029 (2018).

28 Khan, A. *et al.* JASPAR 2018: update of the open-access database of transcription factor binding profiles and its web framework. *Nucleic Acids Res* **46**, D260-D266, doi:10.1093/nar/gkx1126 (2018).

665 29 Weirauch, M. T. *et al.* Determination and Inference of Eukaryotic Transcription Factor
666 Sequence Specificity. *Cell* **158**, 1431-1443, doi:10.1016/j.cell.2014.08.009 (2014).

667 30 McLeay, R. C. & Bailey, T. L. Motif Enrichment Analysis: a unified framework and an
668 evaluation on ChIP data. *BMC Bioinformatics* **11**, 165, doi:10.1186/1471-2105-11-165
669 (2010).

670 31 Miao, Q. *et al.* Tcf3 promotes cell migration and wound repair through regulation of
671 lipocalin 2. *Nat Commun* **5**, 4088, doi:10.1038/ncomms5088 (2014).

672 32 Wagner, K. D. *et al.* The Wilms' tumor gene Wt1 is required for normal development of
673 the retina. *EMBO J* **21**, 1398-1405, doi:10.1093/emboj/21.6.1398 (2002).

674 33 Grant, C. E., Bailey, T. L. & Noble, W. S. FIMO: scanning for occurrences of a given
675 motif. *Bioinformatics* **27**, 1017-1018, doi:10.1093/bioinformatics/btr064 (2011).

676 34 Chandran, V. *et al.* A Systems-Level Analysis of the Peripheral Nerve Intrinsic Axonal
677 Growth Program. *Neuron* **89**, 956-970, doi:10.1016/j.neuron.2016.01.034 (2016).

678 35 Herdegen, T. *et al.* Expression of JUN, KROX, and CREB transcription factors in
679 goldfish and rat retinal ganglion cells following optic nerve lesion is related to axonal
680 sprouting. *J Neurobiol* **24**, 528-543, doi:10.1002/neu.480240410 (1993).

681 36 Herdegen, T., Tolle, T. R., Bravo, R., Zieglgansberger, W. & Zimmermann, M.
682 Sequential expression of JUN B, JUN D and FOS B proteins in rat spinal neurons:
683 cascade of transcriptional operations during nociception. *Neurosci Lett* **129**, 221-224
684 (1991).

685 37 Herman, P. E. *et al.* Highly conserved molecular pathways, including Wnt signaling,
686 promote functional recovery from spinal cord injury in lampreys. *Sci Rep* **8**, 742,
687 doi:10.1038/s41598-017-18757-1 (2018).

688 38 Kenney, A. M. & Kocsis, J. D. Peripheral axotomy induces long-term c-Jun amino-
689 terminal kinase-1 activation and activator protein-1 binding activity by c-Jun and junD in
690 adult rat dorsal root ganglia In vivo. *J Neurosci* **18**, 1318-1328 (1998).

691 39 Leah, J. D., Herdegen, T. & Bravo, R. Selective expression of Jun proteins following
692 axotomy and axonal transport block in peripheral nerves in the rat: evidence for a role in
693 the regeneration process. *Brain Res* **566**, 198-207, doi:10.1016/0006-8993(91)91699-2
694 (1991).

695 40 Ruff, C. A. *et al.* Neuronal c-Jun is required for successful axonal regeneration, but the
696 effects of phosphorylation of its N-terminus are moderate. *Journal of neurochemistry*
697 **121**, 607-618, doi:10.1111/j.1471-4159.2012.07706.x (2012).

698 41 Mahar, M. & Cavalli, V. Intrinsic mechanisms of neuronal axon regeneration. *Nat Rev*
699 *Neurosci* **19**, 323-337, doi:10.1038/s41583-018-0001-8 (2018).

700 42 Dixon, J. R. *et al.* Topological domains in mammalian genomes identified by analysis of
701 chromatin interactions. *Nature* **485**, 376-380, doi:10.1038/nature11082 (2012).

702 43 Velasco, S. *et al.* A Multi-step Transcriptional and Chromatin State Cascade Underlies
703 Motor Neuron Programming from Embryonic Stem Cells. *Cell Stem Cell* **20**, 205-217
704 e208, doi:10.1016/j.stem.2016.11.006 (2017).

705 44 Rau, A., Dhara, S. P., Udvadia, A. J. & Auer, P. L. Regeneration Rosetta: An interactive
706 we application to explore regeneration-associated gene expression and chromatin
707 accessibility. *bioRxiv*, doi:https://doi.org/10.1101/632018 (2019).

708 45 Bray, N. L., Pimentel, H., Melsted, P. & Pachter, L. Near-optimal probabilistic RNA-seq
709 quantification. *Nature Biotechnology* **34**, 525-527, doi:10.1038/nbt.3519 (2016).

710 46 Buenrostro, J. D., Wu, B., Chang, H. Y. & Greenleaf, W. J. ATAC-seq: A Method for
711 Assaying Chromatin Accessibility Genome-Wide. *Curr Protoc Mol Biol* **109**, 21 29 21-29,
712 doi:10.1002/0471142727.mb2129s109 (2015).

713 47 Li, H. & Durbin, R. Fast and accurate short read alignment with Burrows-Wheeler
714 transform. *Bioinformatics* **25**, 1754-1760, doi:10.1093/bioinformatics/btp324 (2009).

715 48 Li, H. *et al.* The Sequence Alignment/Map format and SAMtools. *Bioinformatics* **25**,
716 2078-2079, doi:10.1093/bioinformatics/btp352 (2009).

717 49 Zhang, Y. *et al.* Model-based Analysis of ChIP-Seq (MACS). *Genome Biology* **9**,
718 doi:ARTN R137; 10.1186/gb-2008-9-9-r137 (2008).

719 50 Lawrence, M. *et al.* Software for Computing and Annotating Genomic Ranges. *Plos*
720 *Comput Biol* **9**, doi:ARTN e1003118; 10.1371/journal.pcbi.1003118 (2013).

721 51 Bailey, T. L., Johnson, J., Grant, C. E. & Noble, W. S. The MEME Suite. *Nucleic Acids*
722 *Res* **43**, W39-49, doi:10.1093/nar/gkv416 (2015).

723 52 Pimentel, H., Bray, N. L., Puente, S., Melsted, P. & Pachter, L. Differential analysis of
724 RNA-seq incorporating quantification uncertainty. *Nat Methods* **14**, 687-+,
725 doi:10.1038/nmeth.4324 (2017).

726 53 Benjamini, Y. & Hochberg, Y. Controlling the False Discovery Rate - a Practical and
727 Powerful Approach to Multiple Testing. *J R Stat Soc B* **57**, 289-300 (1995).

728 54 Gu, Z., Eils, R. & Schlesner, M. Complex heatmaps reveal patterns and correlations in
729 multidimensional genomic data. *Bioinformatics* **32**, 2847-2849,
730 doi:10.1093/bioinformatics/btw313 (2016).

731 55 Love, M. I., Huber, W. & Anders, S. Moderated estimation of fold change and dispersion
732 for RNA-seq data with DESeq2. *Genome Biol* **15**, 550, doi:10.1186/s13059-014-0550-8
733 (2014).

734 56 Zhu, L. J. *et al.* ChIPpeakAnno: a Bioconductor package to annotate ChIP-seq and
735 ChIP-chip data. *BMC Bioinformatics* **11**, 237, doi:10.1186/1471-2105-11-237 (2010).

736 57 Robinson, J. T. *et al.* Integrative genomics viewer. *Nat Biotechnol* **29**, 24-26,
737 doi:10.1038/nbt.1754 (2011).

738 58 Supek, F., Bosnjak, M., Skunca, N. & Smuc, T. REVIGO summarizes and visualizes
739 long lists of gene ontology terms. *PLoS One* **6**, e21800,
740 doi:10.1371/journal.pone.0021800 (2011).

741